Geochemistry Geophysics Geosystems G3

Article
Volume 12, Number 6
28 June 2011
Q06017, doi:10.1029/2011GC003544
ISSN: 1525-2027

Published by AGU and the Geochemical Society

Current transport versus continental inputs in the eastern Indian Ocean: Radiogenic isotope signatures of clay size sediments

C. Ehlert and M. Frank
IFM-GEOMAR, Leibniz-Institute of Marine Sciences, Wischhofstrasse 1-3, D-24148 Kiel, Germany (cehlert@ifm-geomar.de)

B. A. Haley
IFM-GEOMAR, Leibniz-Institute of Marine Sciences, Wischhofstrasse 1-3, D-24148 Kiel, Germany

Now at COAS, Oregon State University, 104 Ocean Administration Building, Corvallis, Oregon 97331, USA

U. Böniger
Institute of Earth and Environmental Sciences, University of Potsdam, Karl-Liebknecht-Strasse 24, D-14476 Golm, Germany

P. De Deckker
Research School of Earth Sciences, Australian National University, Canberra, ACT 0200, Australia

F. X. Gingele
Formerly at Department of Earth and Marine Sciences, Australian National University, Canberra, ACT 0200, Australia

[1] Analyses of radiogenic neodymium (Nd), strontium (Sr), and lead (Pb) isotope compositions of clay-sized detrital sediments allow detailed tracing of source areas of sediment supply and present and past transport of particles by water masses in the eastern Indian Ocean. Isotope signatures in surface sediments range from −21.5 (εNd), 0.8299 ($^{87}Sr/^{86}Sr$), and 19.89 ($^{206}Pb/^{204}Pb$) off northwest Australia to +0.7 (εNd), 0.7069 ($^{87}Sr/^{86}Sr$), and 17.44 ($^{206}Pb/^{204}Pb$) southwest of Java. The radiogenic isotope signatures primarily reflect petrographic characteristics of the surrounding continental bedrocks but are also influenced by weathering-induced grain size effects of Pb and Sr isotope systems with superimposed features that are caused by current transport of clay-sized particles, as evidenced off Australia where a peculiar isotopic signature characterizes sediments underlying the southward flowing Leeuwin Current and the northward flowing West Australian Current (WAC). Gravity core FR10/95-GC17 off west Australia recorded a major isotopic change from Last Glacial Maximum values of −10 (εNd), 0.745 ($^{87}Sr/^{86}Sr$), and 18.8 ($^{206}Pb/^{204}Pb$) to Holocene values of −22 (εNd), 0.8 ($^{87}Sr/^{86}Sr$), and 19.3 ($^{206}Pb/^{204}Pb$), which documents major climatically driven changes of the WAC and in local riverine particle supply from Australia during the past 20 kyr. In contrast, gravity core FR10/95-GC5 located below the present-day pathway of the Indonesian throughflow (ITF) shows a much smaller isotopic variability, indicating a relatively stable ITF hydrography over most of the past 92 kyr. Only the surface sediments differ significantly in their isotopic composition, indicating substantial changes in erosional sources attributed to a change of the current regime during the past 5 kyr.

Components: 9500 words, 7 figures, 3 tables.

Keywords: Indonesian throughflow; Leeuwin Current; clay sediments; past circulation; radiogenic isotopes; weathering inputs.

Index Terms: 0473 Biogeosciences: Paleoclimatology and paleoceanography (3344, 4900); 1040 Geochemistry: Radiogenic isotope geochemistry; 3022 Marine Geology and Geophysics: Marine sediments: processes and transport.

Received 2 February 2011; **Revised** 27 April 2011; **Accepted** 27 April 2011; **Published** 28 June 2011.

Ehlert, C., M. Frank, B. A. Haley, U. Böniger, P. De Deckker, and F. X. Gingele (2011), Current transport versus continental inputs in the eastern Indian Ocean: Radiogenic isotope signatures of clay size sediments, *Geochem. Geophys. Geosyst.*, *12*, Q06017, doi:10.1029/2011GC003544.

1. Introduction

1.1. Current System

[2] The Indonesian Archipelago is a key area within the global thermohaline circulation system (THC). Surface and intermediate waters from the western Pacific Ocean flow into the eastern Indian Ocean passing through a series of shallow seas between Indonesia and west Australia (Figure 1a). These currents form the Indonesian Throughflow (ITF) which is the main surface return pathway of the THC from the Pacific into the Indian Oceans [*Schmitz*, 1995]. Warm waters with low salinities originating in the ITF are advected west across the Indian Ocean and, eventually, reach the South Atlantic via the Agulhas Current eddies [*Macdonald and Wunsch*, 1996]. Thus, changes in the intensity and volume input of ITF waters have played an important role in influencing the nature of the global THC, heat exchange and both global and regional climatic conditions [*Gordon et al.*, 1992; *Karas et al.*, 2009].

[3] The ITF is characterized by low surface salinities (Figure 2) and elevated surface temperatures [*Godfrey*, 1996], which results in two salinity fronts near 7°S and 10°–14°S (Figure 2). These fronts separate low-salinity waters (the ITF and the South Java Current (SJC)) from high-salinity Indian Ocean waters (Eastern Gyral Current (EGC) and the South Indian Current (SIC)) [*Fieux et al.*, 1996]. The South Java Current (SJC), which flows along the Java shelf break and slope, is highly variable and reverses its direction every six months due to the biannual variation of the monsoonal winds [*Wijffels et al.*, 1996; *Wyrtki*, 1962]. The ITF surface waters diverge westward into the South Equatorial Current (SEC) (Figure 1a) [*Atmadipoera et al.*, 2009], and southward along the coast of west Australia forming the warm, low-salinity Leeuwin Current (LC): a 100–200 m deep and 50–100 km wide current [*Takahashi and Okada*, 2000; *Wells and Wells*, 1994]. Parallel to the LC, the West Australian Current (WAC), which originates in the central and southern Indian Ocean [*Domingues et al.*, 2007; *Wijffels et al.*, 1996], flows northward and also joins the SEC.

[4] This circulation pattern, and especially the LC, is directly influenced by the strength of the ITF, which itself responds to oceanic and climatic dynamics around Australia and the variability of the monsoon regime over Australia and Asia. The Monsoon follows the variability in the position of the Intertropical Convergence Zone (ITCZ) [*Spooner et al.*, 2005], which shifts between a position at 10°–15°N during austral winter and close to north Australia at 10°S during austral summer.

[5] As a result of a sea level drop of up to 125 m during the last glacial period and, in particular, the Last Glacial Maximum (LGM) [*Yokoyama et al.*, 2001], a large portion of the shelves in the Banda and Arafura Seas were exposed to the atmosphere [*De Deckker et al.*, 2003] and the atmospheric and oceanographic circulation patterns were modified [*Chappell et al.*, 1996; *Williams et al.*, 2009]. While the connection between the Pacific and the Indian Oceans was uninterrupted, the vigor of the ITF and, consequently, the LC were most likely greatly reduced due to the decrease in size and number of pathways [*Wang*, 1999; *Zuraida et al.*, 2009]. Indeed, a significant reduction or even complete cessation of the LC with concomitantly increased influence of the WAC along the west Australian shelf has been proposed for the LGM [*Takahashi and Okada*, 2000; *Wells and Wells*, 1994].

1.2. Geology of Indonesia and Australia and Clay Mineral Sources

[6] Australian geology is broadly characterized by several Archaean [*Johnson*, 2005] and Middle

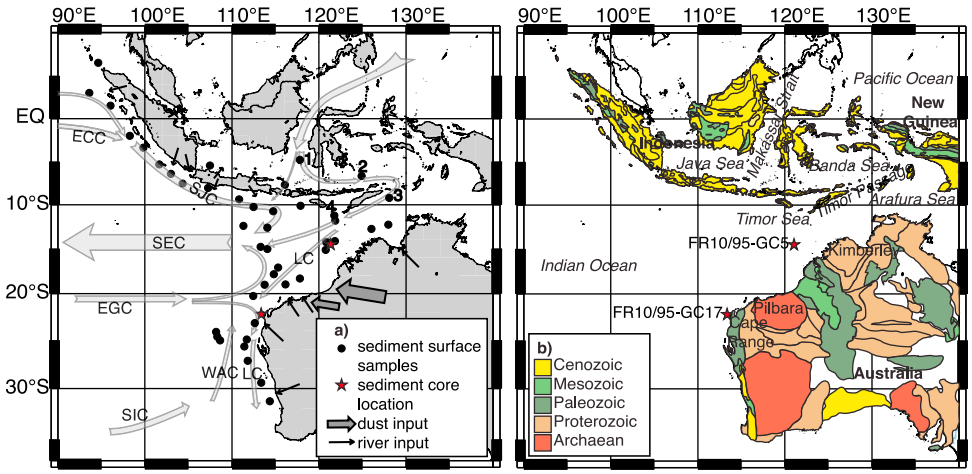

Figure 1. (a) Map showing the sample locations: the 40 surface sediment samples (core tops) used in this study are marked as circles, and the two stars mark the locations of gravity cores FR10/95-GC5 and FR10/95-GC17. The schematic flow patterns of the surface currents have been adopted from *Wijffels et al.* [1996] and *Gingele et al.* [2001a]: EGC, Eastern Gyral Current; ECC, Equatorial Counter Current; LC, Leeuwin Current; SEC, South Equatorial Current; SIC, South Indian Current; SJC, South Java Current; WAC, West Australian Current. Small black arrows denote areas of riverine inputs following *Gingele et al.* [2001a] and large darkgrey arrows denote the pathways of the main dust trajectories after *Bowler* [1976]. (b) Simplified geological map of the study area summarized after *Hamilton* [1979], *Barber and Crow* [2003], and *Johnson* [2005]. The numbers 1 to 4 indicate the surface samples underlying the main pathway of the ITF.

Proterozoic cratons [*Vroon et al.*, 1995]. Permo-Carboniferous glacial sediments are found in the Pilbara and Yilgarn region [*Johnson*, 2005] (Figure 1b) and younger formations of Phanerozoic age occur mainly in north Australia [*Hamilton*, 1979]. The weathering regime of continental Australia has been dominated by continuous erosion accompanied by intense weathering and chemical alteration.

[7] Indonesia, on the other hand, is characterized by the collisional complexes of the Sunda/Banda Arcs, and the passive Australian continental margin, reflecting the complex tectonic interactions between the Indian-Australian and the New Guinea/Bird's Head plates [*Hartono*, 1990; *Vroon et al.*, 1995]. As a consequence, the Indonesian islands mainly consist of Tertiary to Quaternary volcanic rocks (Figure 1b). The only significant exception is northern and central Sumatra, where Early to Middle Carboniferous basement rocks are exposed. West New Guinea also contributes to the sediment supply of the Timor Sea and is characterized by Paleozoic to Mesozoic rocks (Figure 1b) [*Hamilton*, 1979; *Vroon et al.*, 1995].

[8] The geochemical signature of the clay size fraction of continent-derived particulates varies as a function of the prevailing lithologies. These fine particles can be efficiently advected over wide distances via ocean currents and in windborne dust. Thus, in principle, clay mineral composition should be a useful tracer of source areas of sediment supply and a proxy for oceanic current strength and direction [*Ehrmann et al.*, 2007; *Fagel et al.*, 1997; *Petschick et al.*, 1996]. As *Gingele et al.* [2001a] demonstrated, the eastern Indian Ocean is a particularly suitable area for the application of clay mineral compositions as a Late Quaternary provenance tracer due to large differences in source rocks and lithologies on the adjacent continental landmasses. On the other hand, *Thiry* [2000]

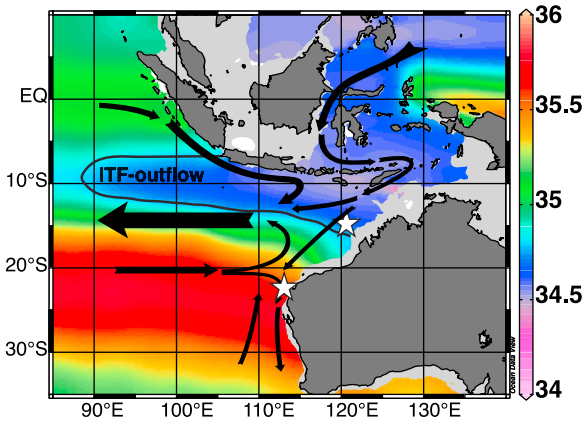

Figure 2. Salinity at 200 m water depth (psu); data source: *Antonov et al.* [2006]. The stars indicate the location of the cores, and the black arrows indicate the main surface circulation as described in Figure 1a.

pointed out that clay mineral assemblages do not provide information about changes in weathering over short time scales such as glacial-interglacial stages. For example, Australia has had a long and complex history of intense surface weathering, resulting in ambiguous modern and late Quaternary marine sediments clay assemblage data around Australia that appear to have no climatic significance [*Gingele et al.*, 2001b; *Thiry*, 2000].

[9] Here, we use the radiogenic isotope compositions (neodymium (Nd), strontium (Sr), lead (Pb)) of the clay fraction of marine sediments to trace present and past current pathways and water mass mixing, as well as continental inputs in the eastern Indian Ocean [*Dia et al.*, 1992; *Fagel et al.*, 2004; *Franzese et al.*, 2009]. Radiogenic isotopes are a powerful tool for this purpose, because the source rocks have a characteristic isotopic fingerprint as a function of rock type and age [*Goldstein et al.*, 1984], attributes that vary widely among the source rocks in the ITF region [*Dia et al.*, 1992; *Jeandel et al.*, 1998; *Vroon et al.*, 1995].

[10] Similar to mineralogical assemblage data, the radiogenic Nd, Sr and Pb isotope systems can become decoupled from the parent rock signatures during weathering and erosion processes. For example, labile Sr and Pb initially released from granitoid weathering are often more radiogenic in their isotopic compositions than the corresponding whole rock values. In the case of Pb, this is due to the damage of the crystal structure of the minerals due to α recoil during radioactive decay of the U series isotopes. In the case of Sr, preferential dissolution of labile minerals with highly radiogenic isotope compositions is usually responsible for any observed fractionation [*Erel et al.*, 1994; *Harlavan et al.*, 1998]. Nd, which is more concentrated in weathering-resistant minerals, is either released unaltered or with a less radiogenic isotope signature than the bulk parent rocks [*Andersson et al.*, 2001]. These differences are most evident during weathering of freshly exposed granitic rocks. In contrast, rocks (i.e., soils) that have experienced a long history of weathering generate secondary minerals (e.g., clays) with isotopic signatures similar to the bulk parent material [*von Blanckenburg and Nägler*, 2001]. Weathering processes can also create sorting effects between minerals of varying resistivity against weathering. This may lead to grain size sorting of the weathering products, and result in variable isotopic compositions that are difficult to unambiguously relate to the isotopic composition of the source rocks. Despite these potential long-term influences on the isotopic composition of weathered materials (i.e., clays), the isotopic composition of the clay size fraction supplied from a particular region is not expected to change on the relatively short glacial/interglacial time scales. This is due to the overall long-term constancy of the weathering conditions in the study area and renders the radiogenic isotope composition of the clay fraction a prospective tracer for weathering sources and past ocean current transport.

[11] Although the goal of this study is mainly to document the potential of the radiogenic isotope composition of the clay size fraction of the sediments to trace the main current systems in the eastern Indian Ocean, we also present two relatively coarse resolution palaeorecords in order to demonstrate the high sensitivity of this method to detect past changes in erosional inputs and ocean circulation.

2. Material

[12] A total of 40 core top samples were analyzed covering the Indonesian Island Arc from Sumatra to the Arafura Sea and the area offshore the northwest and west coast of Australia (Figure 1 and Table 1). The sediments were recovered during two cruises with RV *Baruna Jaya* in 1990, and during two cruises with RV *Franklin* in 1995 and 1996. Aliquots of the same samples were used in a previous study on the clay mineral composition [*Gingele et al.*, 2001a]. During the RV *Franklin* cruise in 1995, two gravity cores FR10/95-GC5 and FR10/95-GC17 were retrieved offshore northwest Australia. FR10/95-GC5 was recovered at 14°00.55′S and 121°01.58′E in 2452 m water depth off northwest Australia, halfway between Timor and North West Cape. The core is undisturbed and covers the past 92 kyr. FR10/95-GC17 was taken 60 km west of the Cape Range Peninsula at 22°07.74′S and 113°30.11′E at a water depth of 1093 m. There is no evidence of significant reworking or depositional disturbances over the past 45 kyr. The core site is located underneath the pathway of aeolian dust from the Australian hinterland to the eastern Indian Ocean.

[13] The age model of core FR10/95-GC17 is based on the $\delta^{18}O$ record of *Globigerinoides sacculifer* [*Martinez et al.*, 1999], and was later supported by 15 AMS ^{14}C and several OSL dates [*van der Kaars and De Deckker*, 2002; *Olley et al.*, 2004]. This results in a detailed chronostratigraphy yielding

Table 1. Radiogenic Isotope Data of Eastern Indian Ocean Clay Size Surface Sediments[a]

Sample	Latitude	Longitude	Depth (m)	Age (yr)	$^{143}Nd/^{144}Nd$	$1\sigma_{(SD)}$	εNd	$^{87}Sr/^{86}Sr$	$1\sigma_{(SD)}$	$^{208}Pb/^{204}Pb$	$^{207}Pb/^{204}Pb$	$^{206}Pb/^{204}Pb$
SHIP-9001	06°11.57′S	103°11.80′E	1348		0.512411	±12	−4.4	0.714707	±7	37.78	15.59	17.81
SHIP-9005	07°26.97′S	116°16.98′E	472		0.512411	±5	−4.4	0.708796	±10	37.68	15.57	17.76
SHIP-9006	04°33.22′S	117°59.58′E	1999		0.512414	±8	−4.4	0.712770	±7	37.50	15.54	17.58
SHIP-9013	06°25.76′S	125°05.24′E	1850		0.512299	±10	−6.6	0.715637	±7	38.31	15.60	18.26
SHIP-9017	08°59.55′S	128°16.91′E	3294		0.512197	±9	−8.6	0.724072	±7	38.89	15.67	18.71
SHIP-9020	10°59.35′S	121°58.08′E	2556		0.512123	±5	−10.1	0.725821	±9	39.11	15.68	18.84
SHIP-9022	11°35.44′S	122°03.80′E	2313		0.512170	±10	−9.1	0.728248	±5	38.75	15.66	18.57
SHIP-9026	09°52.96′S	118°05.53′E	2466		0.512404	±9	−4.6	0.712598	±6	37.72	15.56	17.79
SHIP-9028	10°31.43′S	114°57.35′E	2107		0.512596	±9	−0.8	0.707861	±6	38.53	15.66	18.29
SHIP-9033	10°01.40′S	112°41.40′E	2434		0.512027	±9	−11.9	0.706863	±7	37.83	15.55	17.66
SHIP-9034	09°09.70′S	111°00.70′E	3330		0.512596	±8	−0.8	0.708083	±7	38.26	15.60	18.17
SHIP-9040	07°41.20′S	107°27.30′E	700		0.512673	±10	0.7	0.708030	±7	38.08	15.61	17.96
SHIP-9043	07°19.57′S	104°32.65′E	3331		0.512433	±8	−4.0	0.714732	±6	38.26	15.62	18.19
SHIP-9048	05°32.15′S	107°39.58′E	43		0.512218	±11	−8.2	0.724718	±6	38.46	15.64	18.32
GC-95/1	12°02.34′S	128°09.17′E	124		0.511785	±6	−16.6	0.782428	±10	40.32	15.83	19.89
GC-95/2	12°32.86′S	126°14.84′E	81		0.511849	±9	−15.4	0.737069	±6	39.43	15.75	19.21
GC-95/4	13°55.18′S	122°01.51′E	470		0.512008	±9	−12.3	0.754659	±6	39.13	15.72	18.98
GC-95/5	14°00.55′S	121°01.58′E	2472		0.512016	±6	−12.1	0.741978	±10	39.32	15.73	19.11
GC-95/6	14°19.67′S	121°09.81′E	2177	1390 ± 45	0.511948	±7	−13.5	0.749859	±10	39.56	15.76	19.26
GC-95/8	14°54.97′S	120°57.49′E	678		0.511924	±8	−13.9	0.768210	±6	39.20	15.73	18.98
GC-95/9	18°07.63′S	118°00.92′E	498		0.511896	±8	−14.5	0.759401	±6	38.87	15.70	18.75
GC-95/11	17°38.57′S	114°59.93′E	2458	3010 ± 60	0.511970	±10	−13.0	0.764089	±6	38.97	15.72	18.84
GC-95/13	18°49.26′S	113°58.26′E	1454	2310 ± 50	0.511813	±5	−16.1	0.779594	±9	-	-	-
GC-95/14	20°02.71′S	112°39.73′E	997		0.511772	±15	−16.9	0.798278	±6	39.18	15.79	19.14
GC-95/18	22°59.64′S	112°49.86′E	1055		0.511535	±5	−21.5	0.829902	±11	39.02	15.76	19.06
GC-95/20	24°44.67′S	111°49.75′E	841	2800 ± 60	0.511785	±9	−16.6	0.779592	±6	38.86	15.72	18.76
GC-95/21	25°59.78′S	111°38.09′E	982		0.512212	±4	−8.3	0.739501	±9	-	-	-
GC-95/22	26°59.52′S	112°00.31′E	1049		0.511797	±11	−16.4	0.766405	±8	38.91	15.72	18.77
GC-95/26	29°14.42′S	113°33.48′E	1738	2560 ± 35	0.511777	±8	−16.8	0.755731	±6	38.99	15.72	18.78
GC-96/1	31°06.64′S	114°32.89′E	2530		0.511598	±6	−20.3	0.746042	±11	39.17	15.73	19.17
GC-96/8	24°50.76′S	108°49.48′E	2670	1315 ± 50	0.512210	±5	−8.4	0.718911	±9	38.96	15.70	18.82
GC-96/10	24°27.85′S	108°30.61′E	2852		0.512034	±12	−11.8	0.735160	±6	38.86	15.71	18.73
GC-96/11	23°57.16′S	108°22.14′E	2404		0.511986	±5	−12.7	0.749585	±9	38.85	15.69	18.75
GC-96/16	12°11.29′S	111°30.45′E	2714		0.512388	±10	−4.9	0.713684	±6	39.15	15.78	19.13
GC-96/19	12°22.76′S	114°16.96′E	3355		0.512232	±11	−7.9	0.717000	±8	38.69	15.66	18.58

Table 1. (continued)

Sample	Latitude	Longitude	Depth (m)	Age (yr)	$^{143}Nd/^{144}Nd$	$1\sigma_{(SD)}$	εNd	$^{87}Sr/^{86}Sr$	$1\sigma_{(SD)}$	$^{208}Pb/^{204}Pb$	$^{207}Pb/^{204}Pb$	$^{206}Pb/^{204}Pb$
GC-96/20	14°34.95'S	113°30.49'E	2497	6070 ± 80	0.512112	±6	−10.3	0.724983	±10	39.13	15.69	18.95
GC-96/21	14°48.68'S	114°16.37'E	2919		0.512177	±16	−9.0	0.724602	±6	38.86	15.68	18.71
GC-96/26	16°54.00'S	115°31.00'E	1958		0.512008	±9	−12.3	0.755995	±9	38.88	15.69	18.78
GC-96/28	18°47.93'S	116°20.23'E	502	1740 ± 50	0.511745	±7	−17.4	0.778866	±9	39.09	15.73	18.75
BARP-9419	03°15.18'N	093°49.08'E	3145		0.511967	±8	−13.1	0.735396	±5	37.14	15.57	17.46
BARP-9424	06°44.40'N	094°50.46'E	2676		0.512174	±5	−9.1	0.717152	±11	37.09	15.55	17.44
BARP-9431	01°44.16'N	096°14.28'E	3235		0.512106	±10	−10.4	0.725692	±7	38.92	15.71	18.64
BARP-9434	01°45.18'S	098°27.54'E	2780		0.512160	±8	−9.3	0.723295	±7	38.29	15.63	18.18
BARP-9440	03°10.14'S	100°01.38'E	1495		0.512219	±11	−8.2	0.721303	±6	38.41	15.65	18.21
BARP-9441	05°06.66'S	101°51.12'E	1099		0.512512	±5	−2.5	0.709935	±9	37.10	15.55	17.44

[a]Uncertainties are $1\sigma_{(SD)}$ internal reproducibilities of the measured isotope ratios. All ages listed are AMS ^{14}C dates, measured on *G. ruber* (P. De Deckker, unpublished data, 2001).

sedimentation rates between 2.8 and 19.2 cm/kyr and an age of 46 ka at 240 cm core depth. We analyzed samples from the upper 160 cm of core FR10/95-GC17 which corresponds to the past 25 kyr. For core FR10/95-GC5, a combination of $\delta^{18}O$ records of *Globigerinoides sacculifer* for the upper 93 cm, and *Globigerinoides ruber* below 93 cm was tuned to SPECMAP to establish the stratigraphy [*Gingele et al.*, 2001b]. To achieve consistency between the isotopic records obtained from two different species with different dwelling habitats, a value of 1‰ was subtracted from all $\delta^{18}O$ values of *Globigerinoides ruber*. Individual isotope events were identified by comparison with the SPECMAP stack and tagged with the respective ages provided by *Gingele et al.* [2001b] and *Martinson et al.* [1987]. The average sedimentation rate is about 2.8 cm/kyr. For this study, samples of the uppermost 290 cm were analyzed, which corresponds to a maximum age of 92 ka.

3. Analytical Methods

[14] Sediment samples were treated with hydrogen peroxide (10%) and acetic acid (10%) at room temperature to remove organic matter and carbonates and to disaggregate the clay minerals. No further treatment to remove ferromanganese coatings was performed because potential alteration of the isotopic results is unlikely in view of the high concentrations in Nd, Sr and Pb in the terrigenous sediments. Subsequently, the clay size fraction (<2 μm) was separated by conventional settling techniques [*Gingele et al.*, 2001a]. Unfortunately, due to analytical problems with the available clay size samples, the Pb isotope data for core FR10/95-GC17 had to be obtained on bulk sediment. After complete dissolution in a mixture of concentrated HF-HNO_3, Pb, Sr and Nd were separated and purified for mass spectrometric analyses by application of standard ion chromatographic procedures [*Cohen et al.*, 1988; *Horwitz et al.*, 1992; *Lugmair and Galer*, 1992].

[15] All radiogenic isotope measurements were performed on a Nu Instruments MC-ICPMS at IFM-GEOMAR in Kiel. Measured Nd isotopic compositions were corrected for instrumental mass bias using a $^{146}Nd/^{144}Nd$ of 0.7219. External reproducibility was estimated by repeated measurements of the JNdi-1 standard and was always better than 42 ppm ($2\sigma_{(SD)}$). All Nd isotope ratios were normalized to the accepted literature value for JNdi-1 of 0.512115 [*Tanaka et al.*, 2000]. Nd isotope data are expressed as εNd values, which

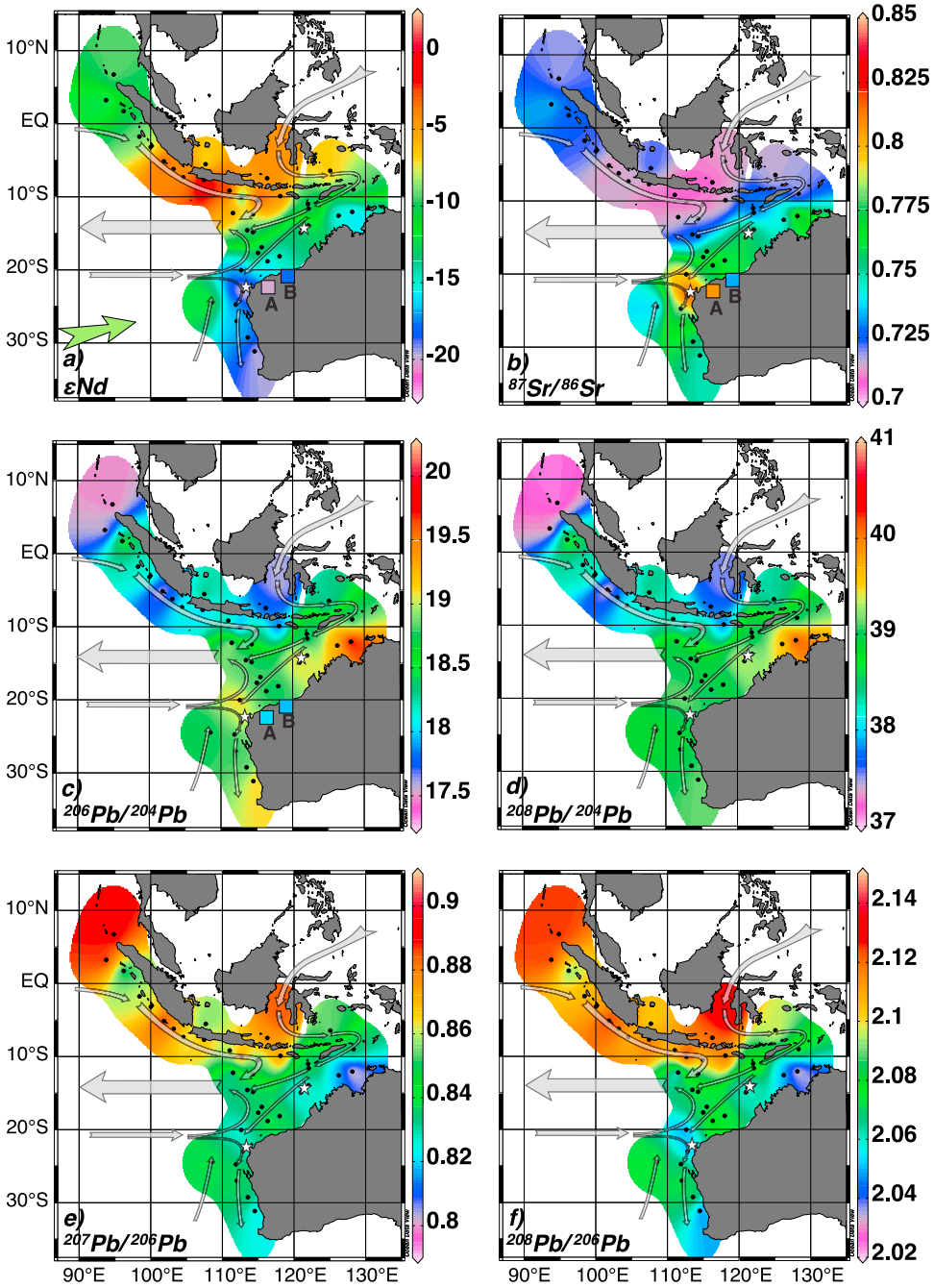

Figure 3. Isotopic composition of the clay-sized surface sediments in the eastern Indian Ocean: (a) εNd, (b) $^{87}Sr/^{86}Sr$, (c) $^{206}Pb/^{204}Pb$, (d) $^{208}Pb/^{204}Pb$, (e) $^{207}Pb/^{206}Pb$, and (f) $^{208}Pb/^{206}Pb$. Black dots and white stars indicate the sample and core locations, respectively. The plots were generated using ODV software, version 3.4.0 (R. Schlitzer, Ocean Data View, 2008, available at http://odv.awi.de). The color of the arrow in Figure 3a indicates an εNd = −7.7, measured by *Dia et al.* [1992] for sediments underlying the SIC at 28.535°S, 85.463°E. The squares indicate measurements of dust samples A: 22°54.3′S, 114°46.957′E, εNd = −20.1, $^{87}Sr/^{86}Sr$ = 0.8112, $^{206}Pb/^{204}Pb$ = 18.014 and B: 19°47.385′S, 120°40.557′E, εNd = −17.9, $^{87}Sr/^{86}Sr$ = 0.7328, $^{206}Pb/^{204}Pb$ = 17.9352. The light gray arrows indicate the main surface circulation as described in Figure 1a.

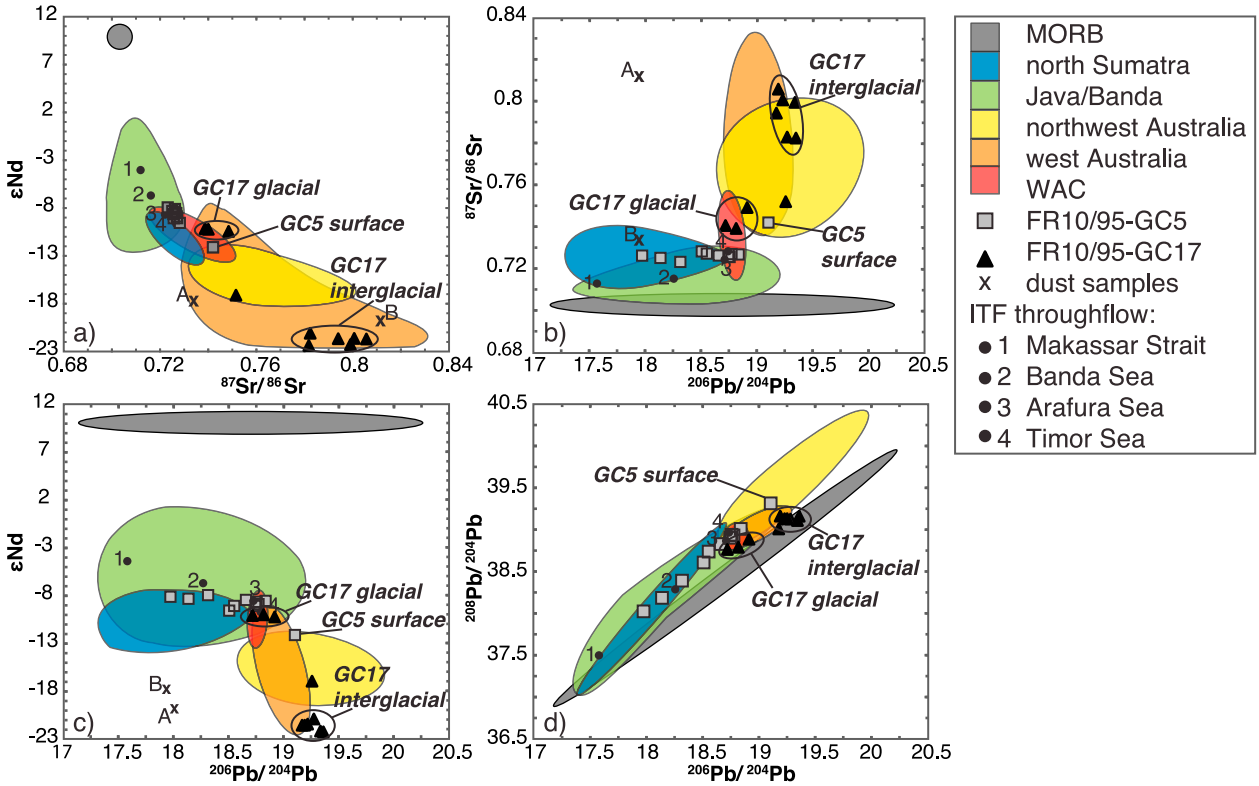

Figure 4. (a) The εNd-$^{87}Sr/^{86}Sr$, (b) $^{87}Sr/^{86}Sr$-$^{206}Pb/^{204}Pb$, (c) εNd-$^{206}Pb/^{204}Pb$, and (d) $^{208}Pb/^{204}Pb$-$^{206}Pb/^{204}Pb$ systematics for the clay-sized eastern Indian Ocean sediments and the two cores FR10/95-GC5 and FR10/95-GC17. Error bars are smaller than symbol size. Approximate MORB signatures are given for comparison. The colored areas mark distinct areas of similar isotope values in the clay-sized surface sediments. A and B for the dust samples are the same as in Figure 3. The numbers 1 to 4 indicate the surface samples underlying the main pathway of the ITF.

denote the deviation of the measured $^{143}Nd/^{144}Nd$ ratio from the chondritic uniform reservoir CHUR (0.512638), multiplied by 10,000.

[16] The measured $^{87}Sr/^{86}Sr$ ratios were corrected for instrumental mass bias using $^{88}Sr/^{86}Sr = 8.3752$ and were normalized to the accepted value for NIST SRM987 of 0.710245. The 2σ external reproducibility of repeated standard measurements was 64 ppm.

[17] For Pb isotope measurements, a standard sample bracketing method was applied [*Elburg et al.*, 2005], during which one standard was run every five samples. The sample ratios were normalized to the accepted ratios of NIST SRM-981 of 36.7219 ($^{208}Pb/^{204}Pb$), 15.4936 ($^{207}Pb/^{204}Pb$), and 16.9405 ($^{206}Pb/^{204}Pb$), respectively, as given by *Abouchami et al.* [1999]. The 2σ external reproducibilities for repeated standard measurements applying the above bracketing technique were relatively high (1348 ppm for $^{208}Pb/^{204}Pb$; 1024 ppm for $^{207}Pb/^{204}Pb$; 680 ppm for $^{206}Pb/^{204}Pb$), but, in light of the range of the Pb data of the samples, this precision was fully sufficient.

[18] The internal precision of each sample and each standard measurement was always better than the external reproducibility. Error bars shown on the figures correspond to the 2σ external reproducibilities listed, and are generally smaller than the symbol size of the data points. The data are available via the Pangaea database (www.pangaea.de).

4. Results

4.1. Radiogenic Isotope Distribution in the Surface Sediments

[19] All isotope systems show a large range of values (Figures 3 and 4). A sharp isotopic boundary is found between 10° and 14°S, separating the Australian shelf from the Indonesian region. Highly radiogenic εNd and unradiogenic Sr and Pb isotope ratios are found in samples around Java and

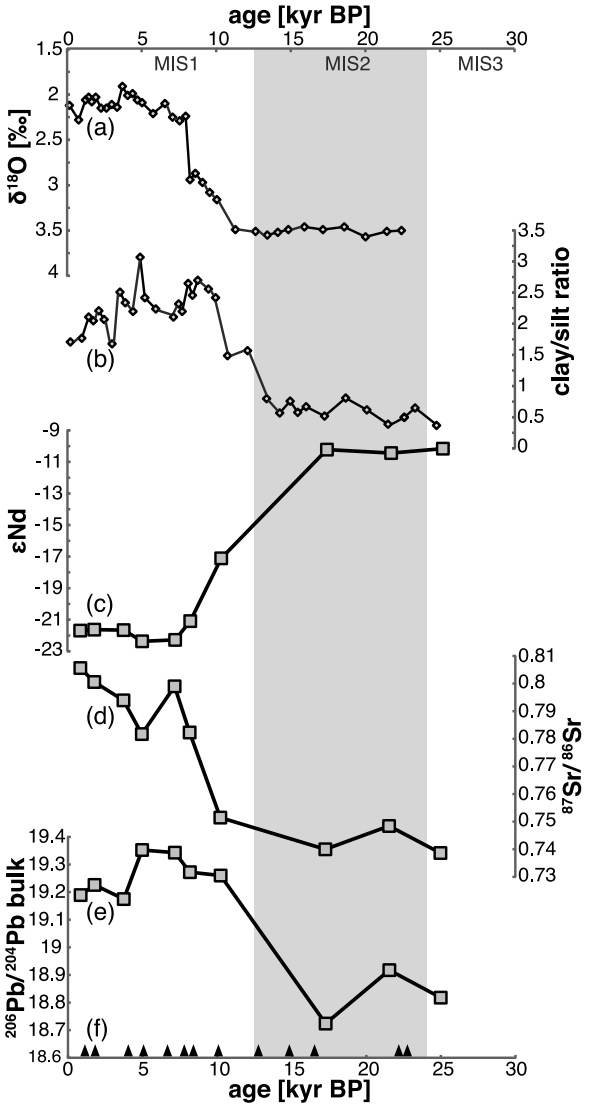

Figure 5. Time series for core FR10/95-GC17, (a) $\delta^{18}O$, and (b) clay/silt ratio [*Gingele et al.*, 2001b], (c) εNd, (d) $^{87}Sr/^{86}Sr$, and (e) $^{206}Pb/^{204}Pb_{bulk}$ versus age. Error bars are smaller than symbol size. Marine Isotope Stages were assigned according to the SPECMAP chronology [*Martinson et al.*, 1987], supported by 15 AMS ^{14}C ((f) indicated by black triangles) and several OSL dates [*van der Kaars and De Deckker*, 2002; *Olley et al.*, 2004].

Sumatra, whereas unradiogenic εNd and radiogenic Sr and Pb isotope ratios are characteristic for samples off northwest and west Australia. εNd ranges from −21.5 off Cape Range in northwest Australia to +0.7 south of Java, Sr isotope values reach from 0.7069 south of Java to 0.8299 northwest of the Cape Range Peninsula. The $^{208}Pb/^{204}Pb$, $^{207}Pb/^{204}Pb$ and $^{206}Pb/^{204}Pb$ ratios range from 37.09 to 40.32, from 15.55 to 15.83 and from 17.44 to 19.89, respectively. The region off northern and central Sumatra is characterized by intermediate εNd values around −10 and unradiogenic $^{87}Sr/^{86}Sr$ ratios around 0.72 but varying Pb isotope ratios. The least radiogenic Pb isotope ratios are found close to the northern tip of Sumatra and around southern Sumatra. The surface sediments underlying the main ITF pathway through the Timor Passage are characterized by gradually decreasing εNd and increasing Sr and Pb isotope values (Figures 3 and 4). All isotope systems show prominent regional signatures with low εNd and high Sr and Pb isotope ratios off the Kimberley coast in north Australia and off southwest Australia. Further offshore, below the WAC, the samples show intermediate Nd, Sr and Pb isotope signatures.

4.2. Late Quaternary Evolution of the Radiogenic Isotope Compositions

[20] The record of core FR10/95-GC17, situated directly below the present-day path of the LC, covers the past 25 kyr (Figure 5 and Table 2). Prior to 17 ka the εNd signature of the clay sediments was essentially constant at −10. Between 17 and 8 ka, a large shift to more unradiogenic values around −22 occurred and has remained at this value until the present day, which is consistent with the present-day surface value in the area. The $^{87}Sr/^{86}Sr$ and $^{206}Pb/^{204}Pb$ records show inversely correlating patterns, with relatively unradiogenic Sr (~0.74) and Pb (~18.8) prior to 17 ka, followed by a shift toward more radiogenic Sr (~0.8) and Pb (19.3) between 17 and 10 ka, which are also similar to today's surface values in this area.

[21] Core FR10/95-GC5 is located halfway between Timor and the North West Cape, under the main flow path of the ITF. The record of core GC5 covers the past 92 kyr (Figure 6 and Table 3) and thus extends back into the end of the penultimate interglacial. The resolution of this record is lower than that of core GC17 and the range of isotopic variability is also much smaller. The εNd values range from −9.6 in the part of the record corresponding to the end of MIS 5a [*Martinson et al.*, 1987] to −8 in the mid Holocene. Correspondingly, $^{87}Sr/^{86}Sr$ signatures only vary between 0.72 in the youngest sample and 0.73 at 80 ka. In contrast, the surface sample is much less radiogenic in Nd (εNd = −13.5) and more radiogenic in Sr isotopes (0.75). The Pb isotope signature ranges between 17.97 and 18.84 for $^{206}Pb/^{204}Pb$, whereby the oldest sample is characterized by the most radiogenic ratios. Similar to Nd and Sr isotopes, the

Table 2. Radiogenic Isotope Data of Clay Size Sediments of Core FR10/95-GC17[a]

Sample Depth (cm)	Age (yr)	$^{143}Nd/^{144}Nd$	$1\sigma_{(SD)}$	εNd	$^{87}Sr/^{86}Sr$	$1\sigma_{(SD)}$	$^{208}Pb/^{204}Pb$ Bulk	$^{207}Pb/^{204}Pb$ Bulk	$^{206}Pb/^{204}Pb$ Bulk
5.5	847	0.511526	±5	−21.7	0.805679	±7	39.14	15.79	19.19
25.5	1781	0.511529	±5	−21.6	0.800627	±7	39.11	15.79	19.23
41.5	3739	0.511528	±5	−21.7	0.793983	±6	39.01	15.79	19.18
56.5	4970	0.511491	±5	−22.4	0.781766	±7	39.14	15.82	19.35
70	7166	0.511496	±6	−22.3	0.799058	±6	39.10	15.82	19.34
80.5	8174	0.511557	±7	−21.1	0.782343	±7	39.11	15.81	19.27
98	10233	0.511761	±5	−17.1	0.751519	±6	39.11	15.80	19.26
125.5	17272	0.512114	±6	−10.2	0.740033	±6	38.76	15.66	18.72
137.5	21543	0.512103	±6	−10.4	0.748479	±5	38.88	15.70	18.92
158.5	24986	0.512117	±7	−10.2	0.738691	±7	38.79	15.70	18.82

[a]Uncertainties are $1\sigma_{(SD)}$ internal reproducibilities of the measured isotope ratios. The age model is based on the $\delta^{18}O$ record of *G. sacculifer* [*Martinez et al.*, 1999] supported by 15 AMS ^{14}C dates [*van der Kaars and De Deckker*, 2002; *Olley et al.*, 2004].

surface sample shows a value different from the rest of the record (19.26).

5. Discussion

5.1. Surface Sediment Provenance and Ocean Circulation Patterns

[22] The three isotope systems provide information for clear distinction of three main source areas of the clay size sediments (north Sumatra, Java/Banda, and northwest/west Australia), as well as for the ocean current transport mechanisms that control the clay distributions. Comparison with the clay mineralogy data presented by *Gingele et al.* [2001a] shows overall similarities but also important differences.

[23] All three isotope systems show largely similar but in some cases distinct surface sediment patterns (Figures 3 and 4). This indicates that long-term weathering processes in the different source areas have led to some decoupling of Nd, Sr and Pb isotope signatures of the fine-grained sediments (e.g., incongruent weathering of rocks with distinct isotopic signatures of the rock-forming minerals and grain size sorting [*von Blanckenburg and Nägler*, 2001]). This does, however, not diminish the potential of combined radiogenic isotope compositions of the clay size sediments as tracers for provenance and surface and subsurface currents in the study area but, on the contrary, adds valuable additional information. It is noted here that it is not possible to distinguish transport by surface and deep currents or sediment redistribution by bottom currents on the basis of the radiogenic isotope signatures of the clay size sediments. However, today prevailing surface and subsurface currents in the area are strongest. Similar to the situation around Indonesia and northwest Australia, the area south of Africa is also characterized by strong surface circulation and the underlying sediments reflect that [*Franzese et al.*, 2009]. It is thus assumed that the observed isotopic variability is mainly influenced by surface and subsurface currents.

5.1.1. Isotopic Composition and Mineralogy of Potential Regional Sediment Sources

[24] The ability to trace circulation using the radiogenic isotopes clearly depends on compositional variations in the sources of the clays. The question then faced is to what extent the observed isotopic variations in the surface sediments reflect circulation versus clay source variability? The isotopic signatures, as well as clay mineralogy of the sediments around north Sumatra, indicate that these clays are dominated by local input that reflects hinterland geology. These sediments are sharply separated from the area around Java/Banda (Figures 4 and 7). This is consistent with the Early to Middle Carboniferous [*Barber and Crow*, 2003] basement rocks of north and central Sumatra as the dominant source for the fine-grained sediments, which is in distinct contrast to the Tertiary to Quaternary source rocks for sediments of south Sumatra and Java/Banda. There is also a clear separation between Indonesian and northwest Australian sediments in their isotopic composition (Figure 4), as well as in direct comparison between the isotopic and clay mineral distribution (Figure 7).

[25] In contrast to the clay mineralogy, the isotopic data indicate no separation between a Central (south Sumatra, Java, Bali and Lombok) and an Eastern Province (Timor and north New Guinea)

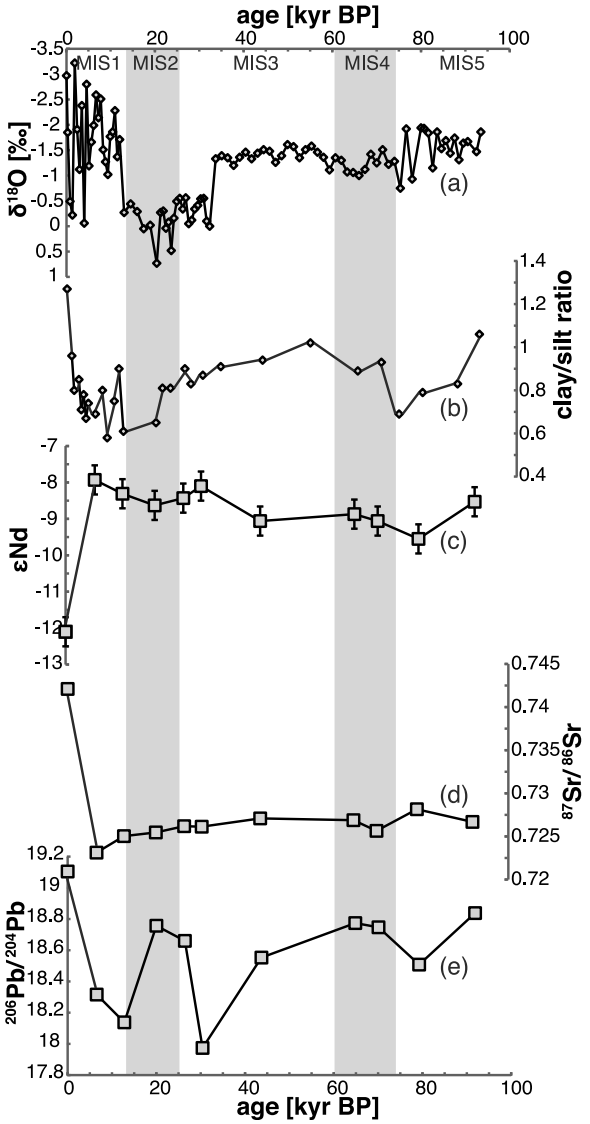

Figure 6. Time series for core FR10/95-GC5, (a) $\delta^{18}O$, and (b) clay/silt ratio [*Gingele et al.*, 2001b], (c) εNd, (d) $^{87}Sr/^{86}Sr$, and (e) $^{206}Pb/^{204}Pb$ versus age. Error bars are either smaller than symbol size or represent $2\sigma_{(SD)}$ external reproducibilities of repeated standard measurements. Marine Isotope Stages were assigned according to the SPECMAP chronology [*Martinson et al.*, 1987]. The broad $\delta^{18}O$ fluctuations during the Holocene are caused by monsoonal rains that are commonly isotopically light and also engender low salinities.

within the Indonesian islands (Figures 4 and 7). Highly radiogenic Nd and unradiogenic Sr isotope signatures indicate the existence of only one sedimentary province that spans the south Sumatra, Timor and Arafura Seas, including the entire area of the Java and Banda Seas within the archipelago, and the Makassar Strait (Figures 3 and 4). Off west Australia the clay mineralogy data of *Gingele et al.* [2001a] indicate dominance of clay transport via the WAC for the entire area, whereas the isotopes clearly distinguish between the influence of west Australia and WAC transport (Figure 4).

[26] These observations demonstrate that the measured radiogenic isotope signatures, reflecting primarily the petrographic signature of the parent bedrock and their thermotectonic evolution, is more informative on provenance than clay and help to define distinct source regions of the clays contained in the surface sediments providing complementary and more specific information than clay mineralogical data alone. With this understanding of the source signatures the spatial distribution of the isotopic data can be compared with oceanic current transport patterns.

5.1.2. Influence of Surface Currents on the Radiogenic Isotope Distribution of the Clay Size Sediments

[27] The sharp isotopic boundaries seen between north Sumatra and Java/Banda in the north and the shelf areas off northwest Australia in the south (Figures 3 and 4) closely mirror surface hydrography associated with the low saline ITF outflow (Figure 2), as well as geological differences (Figure 1b). The westward outflow of the ITF efficiently separates water masses and material transport around Indonesia from that off northwest Australia, thus essentially preventing transport of material between these areas. Comparison between the different isotope systems (Figure 4) indicates that two different source areas for the clays are required to explain the isotopic distributions north and south of this boundary.

[28] Relatively little isotopic variability is observed in the sediments from the Java/Banda Seas. These fine-grained sediments are entrained into the SJC, which reverses its direction semiannually due to changing monsoonal conditions [*Wijffels et al.*, 1996]. As a result, clays are transported both eastward and westward in a biyearly cycle, which precludes development of a distinct isotopic pattern in the underlying sediments.

[29] The pathway of the northern part of the ITF itself is not reflected by a distinct radiogenic isotope signature but, in contrast to the mineralogical distribution [*Gingele et al.*, 2001a], the clay size sediments deposited under the main branch of the ITF display a gradual isotopic transition from the Makassar Strait through the Banda, Arafura and Timor Seas. South of the Timor Seas these changes reflect more Indonesian-like (radiogenic Nd and

Table 3. Radiogenic Isotope Data of Clay Size Sediments of Core FR10/95-GC5[a]

Sample Depth (cm)	Age (yr)	$^{143}Nd/^{144}Nd$	$1\sigma_{(SD)}$	εNd	$^{87}Sr/^{86}Sr$	$1\sigma_{(SD)}$	$^{208}Pb/^{204}Pb$	$^{207}Pb/^{204}Pb$	$^{206}Pb/^{204}Pb$
25	6549	0.512231	±11	−7.9	0.723166	±6	38.39	15.64	18.32
47	12773	0.512212	±12	−8.3	0.725078	±6	38.19	15.62	18.14
57	20008	0.512196	±11	−8.6	0.725505	±7	38.94	15.69	18.76
77	26433	0.512206	±11	−8.4	0.726230	±6	38.83	15.68	18.66
89	30416	0.512223	±9	−8.1	0.726172	±5	38.02	15.62	17.97
129	43692	0.512173	±13	−9.1	0.727132	±6	38.74	15.69	18.55
193	64851	0.512183	±10	−8.9	0.726927	±6	38.93	15.69	18.77
209	70087	0.512174	±10	−9.1	0.725689	±6	38.90	15.68	18.75
237	79250	0.512148	±11	−9.6	0.728196	±6	38.61	15.66	18.51
289	91862	0.512201	±9	−8.5	0.726726	±7	39.01	15.70	18.84

[a]Uncertainties are $1\sigma_{(SD)}$ internal reproducibilities of the measured isotope ratios. The age model is based on a combination of $\delta^{18}O$ records of *G. sacculifer* for the upper 93 cm and *G. ruber* below 93 cm [*Gingele et al.*, 2001b].

unradiogenic Sr and Pb) isotope ratios transitioning into more Australian-like (unradiogenic Nd and radiogenic Sr and Pb) isotope ratios, due to input of clays from Australia and New Guinea (Figures 3 and 4). This interpretation is consistent with the comprehensive study of *Vroon et al.* [1995], in which Pb and, to a lesser extent, Nd isotopes measured in volcanics follows a similar northwest-to-southeast trend. This supports the above observation that the ITF mainly acts as a boundary between different sediment source provenances rather than a conveyor of a particle signature.

[30] For all isotope systems, there is a sharp distinction between the sediments deposited along the

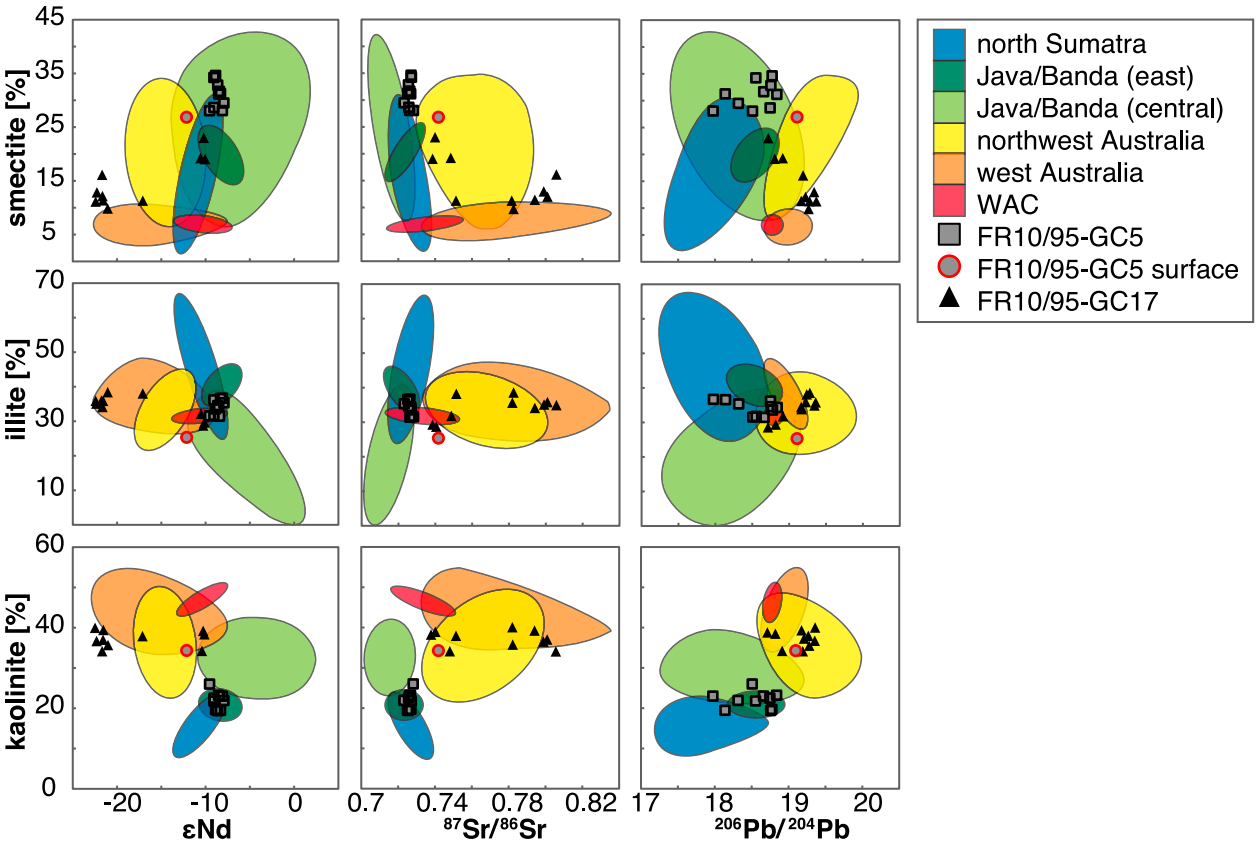

Figure 7. Clay mineral composition versus radiogenic isotope signatures of the clay size sediments for the eastern Indian Ocean sediments and the two cores FR10/95-GC5 and FR10/95-GC17. Error bars are smaller than symbol size. The colored areas are the same as in Figure 4, except for Java/Banda (Eastern) and Java/Banda (Central), which were combined into one group in Figure 4.

coastline of west Australia and those deposited further offshore (Figure 4), whereby sediments deposited directly off the coast and underlying the LC appear to have less radiogenic Nd and more radiogenic Sr and Pb isotope signatures. These isotopic data suggest that clay-sized particles are mostly transported along the coast and that there is very little propagation offshore. The sediments further offshore were most likely transported by the WAC, which originates in the central and southern Indian Ocean [*Domingues et al.*, 2007; *Wijffels et al.*, 1996] and carries clays from distal sources with significantly less radiogenic Sr and Pb and more radiogenic Nd isotope signatures [*Dia et al.*, 1992] compared to the samples closer to the Australian continent (Figure 4).

[31] An anomalous feature are the highly unradiogenic Nd and radiogenic Pb and Sr isotope signatures in sediments off Cape Range in northwest Australia (Figure 3), which cannot be explained by current transport in this region. It is therefore likely that these sediments have been affected by direct input of material from the Pilbara craton in the hinterland (Figure 1b). This sedimentary input most likely mainly occurs via rivers during the wet season or dust during the dry season [*Bowler*, 1976; *Gingele et al.*, 2001a; *Hesse and McTainsh*, 2003]. The latter would be consistent with the major pathway of dust transport from Australia to the eastern Indian Ocean, which crosses the Cape Range area [*Bowler*, 1976] (Figure 1a). Measurements of two samples of dust particles from the respective area show Nd and Sr isotope ratios similar to the surface sediments (Figures 3 and 4). The Pb isotope signatures of the dust particles, in contrast, are more radiogenic than the surface sediments, which is probably due to anthropogenic contamination. Similarly, the isotopic deviations seen in the nearshore sediments off southwest Australia and off the Kimberley coast in north Australia (Figure 3) likely reflect local riverine supply of isotopically distinct clay size sediments.

5.2. Reconstruction of Late Quaternary Changes of the Main Current Systems

[32] Building on the information extracted from the surface distribution of the radiogenic isotopes, the two coarse resolution radiogenic isotope records obtained reveal distinct changes in clay isotopic composition over time, which reflect significant changes in source provenance and regional circulation over the late Quaternary. The most prominent feature in the late Quaternary sediments off west Australia (Core FR10/95-GC17) is a large shift in Nd, Sr and Pb isotopes between 17 and 8 ka (Figure 5). This was a critical period of time representing the last deglaciation and the onset of modern atmospheric and oceanographic circulation [*Harrison*, 1993; *Murgese and De Deckker*, 2007], including the initiation of dominant NW monsoon around 14 ka [*Spooner et al.*, 2005; *Williams et al.*, 2009; *Wyrwoll and Miller*, 2001]. Sediments older than 17 ka are more radiogenic in their Nd isotope composition and less radiogenic in their Sr and Pb isotope composition than today, indicating large changes in sedimentary source provenance. It is unlikely that these older Nd and Sr signatures were the result of changes in "local" inputs of Australian sediments for several reasons: (1) sediments with these isotopic signatures are found in the adjacent continental rocks (Figure 1b), but they are mostly covered by large dune fields and only few river beds and salt lakes near the coast consist of those rocks; (2) any possible riverine input was reduced during the drier glacial period [*Hesse and McTainsh*, 2003; *van der Kaars and De Deckker*, 2002]; and (3) more distal sediment input in the form of dust is not supported by clay/silt ratios (Figure 6) [*Gingele et al.*, 2001b].

[33] Excluding this possible source variability, the most likely explanation for the marked difference of isotope signatures is a different oceanic current regime during the last glacial period: one that was either dominated by the LC or by the WAC. The modern LC in northwest Australia delivers material with signatures of −14 (εNd), 0.77 ($^{87}Sr/^{86}Sr$) and 18.9 ($^{206}Pb/^{204}Pb$), whereas the modern WAC delivers material characterized by signatures of −12 (εNd), 0.74 ($^{87}Sr/^{86}Sr$) and 18.7 ($^{206}Pb/^{204}Pb$) (Figure 3). Data from sediments of the last glacial of core FR10/95-GC17 were more similar to the modern WAC signature than to the samples from underneath the LC off northwest Australia (Figure 4) and thus imply a greater contribution from the former source. This is in agreement with results of several previous studies that found evidence for a weakening of the ITF and the LC during the last glacial [*Gingele et al.*, 2001b; *Zuraida et al.*, 2009]. The decreased current flow from the north was replaced by an increased influence of the WAC on the surface water circulation prior to 14 ka [*Gingele et al.*, 2001b; *Okada and Wells*, 1997; *Wells and Wells*, 1994].

[34] With the onset of the deglaciation the volume transport of the ITF and LC increased [*van der Kaars and De Deckker*, 2002] along with the onset of modern monsoonal circulation. Increased

freshwater runoff and enhanced sediment supply from west Australia caused by higher mean annual rainfall in west and north Australia occurred after 17 ka [*Kawamura et al.*, 2006; *Murgese and De Deckker*, 2007]. The clay/silt ratio indicates a switch to predominantly local input of riverine material, which is reflected by unradiogenic Nd and radiogenic Sr isotope signatures of local continental origin in west Australia after 14–10 ka (Figures 4 and 5). The glacial samples of FR10/95-GC17 have distinctly higher εNd and lower $^{87}Sr/^{86}Sr$ reflecting the influence of the WAC, whereas the younger samples have Nd and Sr ratios characteristic of the local input of Archean material.

[35] Unlike the marginal site FR10/95-GC17, core FR10/95-GC5 located under the main flow path of the ITF only recorded little isotopic variability throughout the last 95 ka (Figure 6). In contrast, the surface sample shows a distinctly different isotope signature. The timing and extent of the isotopic variations of the clay size fraction mirrors the lower clay/silt ratios (coarser material) observed during glacial times that indicate diminished riverine inputs, similar to the situation for core GC17 off west Australia [*Gingele et al.*, 2001b]. The more distal location of core GC5 from the continental sources and its higher water depth were mainly responsible for a weaker amplitude of the changes compared to core GC17. The isotope signatures found throughout the core are on average around −8 (εNd), 0.73 ($^{87}Sr/^{86}Sr$) and 18.6 ($^{206}Pb/^{204}Pb$), which is similar to the signatures of samples from Java/Banda (Figure 4).

[36] In contrast, the isotopic composition of the surface sample of core GC5, which is indistinguishable from the other surface samples in the area, has isotopic ratios of −12 (εNd), 0.74 ($^{87}Sr/^{86}Sr$), and 19.1 ($^{206}Pb/^{204}Pb$), thus plotting within the field defining samples from northwest Australia (Figure 4). The proposed reason for this drastic change is essentially the same as off west Australia. The overall higher aridity in the Australasian region between 14 and 40 ka [*Hesse and McTainsh*, 2003; *van der Kaars et al.*, 2006], less runoff from the Australian continent, and a weaker ITF due to the lower sea level prevented transport of material from the Australian shelves. *Kawamura et al.* [2006] even proposed, that the last interglacial was much drier then the modern. Instead, the environmental conditions off southern Sumatra were relatively stable during the past 133 kyr [*Mohtadi et al.*, 2010]. The eastward flowing SJC was enhanced [*van der Kaars et al.*, 2006; *Wells and Wells*, 1994] and provided larger contributions of fine-grained sediments carrying Indonesian isotope signatures. With the beginning of the deglaciation and of the sea level rise around 18 ka, the Indonesian and Australian shelves were flooded [*De Deckker et al.*, 2003; *Wyrwoll and Miller*, 2001] and the stronger monsoonal and hydrological cycle in northwest Australia allowed enhanced contributions of material from the Arafura Sea and from northwest Australia. This influence is most evident in the surface signatures covering approximately the past 5 kyr, which may suggest that the present-day current regime in the area was not established until 5 ka, when the LC became more prominent [*De Deckker*, 2001].

6. Conclusions

[37] The spatial and temporal variability of surface currents and continental inputs in the eastern Indian Ocean in the vicinity of the Indonesian and Australian shelves was investigated through analyses of the radiogenic isotope compositions of Nd, Sr and Pb in the clay size sediment fraction in order to demonstrate the potential of this approach for reconstructing sediment provenance and surface circulation in the past.

[38] The variability of the isotope data in the surface sediments reflects both the erosional inputs of the adjacent landmasses and surface hydrography and at some locations provides a means for tracing major currents. Clays deposited along the ITF flow path are characterized by a progressive change in isotope ratios due to continuous input of material from the surrounding islands. The southern boundary of the present-day ITF outflow is reflected by sharp changes of the isotopic signatures of the clays because essentially no fine grained material can be transported across the salinity fronts. In contrast, the biannually reversing SJC has homogenized the clay isotope signatures along the southern Java/Banda shelf. Off west Australia, the WAC delivers clays from the central and southern Indian Ocean which have more radiogenic Nd and less radiogenic Sr and Pb isotope signatures than the sediments coming directly off the coast. At a number of locations the radiogenic isotopes in these clay size sediments clearly reflect local input via rivers (north Sumatra, northwest and southwest Australia), as well as dust inputs in the vicinity of the main westward dust trajectory coming from west Australia.

[39] A late Quaternary time series obtained from core FR10/95-GC17 off west Australia documents

a pronounced change from material supplied with the WAC during the last glacial to predominant riverine sources from west Australia during the Holocene. This change occurred between 14 and 10 ka and is in agreement with the development of more humid local conditions since the beginning of the last deglaciation. In contrast, the record of core FR10/95-GC5 located off northwest Australia documents stable hydrographic conditions dominantly reflecting erosional inputs and current transport of clays from Sumatra and Java between 92 ka and about 5 ka. After 5 ka, river supplied and current transported contributions of material from the Arafura Sea and from northwest Australia, and potentially also dust from Australia, became markedly more prevalent and suggest that the present-day current regime in the area was not established until 5 ka. These coarse resolution reconstructions clearly demonstrate that the radiogenic isotope compositions of clay size sediments are a sensitive tool to fingerprint the sources of erosional material and to reconstruct pathways of surface currents in the past ocean.

Acknowledgments

[40] We acknowledge the help of Roland Stumpf, Torben Stichel, and Jutta Heinze in the laboratory of IFM-GEOMAR. The RV *Franklin* cores were obtained during two cruises led by P. De Deckker in 1995 and 1996, respectively, which were funded through access to the Australian National Marine facility and several ARC grants awarded to P. De Deckker. The SHIP and BARP samples were originally provided to P. De Deckker courtesy of F. Guichard. The radiocarbon dates presented herewith were obtained through AINSE grants (99/21 and 06/18) awarded to P. De Deckker. The measurements of the Australian dust samples were performed by Marc Norman. We are thankful to Viviane Bout-Roumazeilles and one anonymous reviewer for the reviews of the manuscript and to Joel Baker for the editorial review of the paper.

References

Abouchami, W., S. J. G. Galer, and A. Koschinsky (1999), Pb and Nd isotopes in NE Atlantic Fe–Mn crusts: Proxies for trace metal paleosources and paleocean circulation, *Geochim. Cosmochim. Acta*, *63*(10), 1489–1505, doi:10.1016/S0016-7037(99)00068-X.

Andersson, P. S., R. Dahlqvist, J. Ingri, and Ö. Gustafsson (2001), The isotopic composition of Nd in a boreal river: A reflection of selective weathering and colloidal transport, *Geochim. Cosmochim. Acta*, *65*(4), 521–527, doi:10.1016/S0016-7037(00)00535-4.

Antonov, J. I., R. A. Locarnini, T. P. Boyer, A. V. Mishonov, and H. E. Garcia (2006), *World Ocean Atlas 2005*, vol. 2, *Salinity*, *NOAA Atlas NESDIS*, vol. 62, edited by S. Levitus, 182 pp., NOAA, Silver Spring, Md.

Atmadipoera, A., R. Molcard, G. Madec, S. E. Wijffels, J. Sprintall, A. Koch-Larrouy, I. Jaya, and A. Supangat (2009), Characteristics and variability of the Indonesian throughflow water at the outflow straits, *Deep Sea Res., Part I*, *56*(11), 1942–1954, doi:10.1016/j.dsr.2009.06.004.

Barber, A. J., and M. J. Crow (2003), An evaluation of plate tectonic models for the development of Sumatra, *Gondwana Res.*, *6*(1), 1–28, doi:10.1016/S1342-937X(05)70642-0.

Bowler, J. M. (1976), Aridity in Australia: Age, origins and expression in aeolian landforms and sediments, *Earth Sci. Rev.*, *12*, 279–310, doi:10.1016/0012-8252(76)90008-8.

Chappell, J., A. Omura, T. Esat, M. T. McCulloch, J. Pandolfi, Y. Ota, and B. Pillans (1996), Reconciliation of late Quaternary sea levels derived from coral terraces at Huon Peninsula with deep sea oxygen isotope records, *Earth Planet. Sci. Lett.*, *141*, 227–236, doi:10.1016/0012-821X(96)00062-3.

Cohen, A. S., R. K. O'Nions, R. Siegenthaler, and W. L. Griffin (1988), Chronology of the pressure-temperature history recorded by a granulite terrain, *Contrib. Mineral. Petrol.*, *98*, 303–311, doi:10.1007/BF00375181.

De Deckker, P. (2001), Late Quaternary cyclic aridity in tropical Australia, *Palaeogeogr. Palaeoclimatol. Palaeoecol.*, *170*, 1–9, doi:10.1016/S0031-0182(01)00233-4.

De Deckker, P., N. J. Tapper, and S. van der Kaars (2003), The status of the Indo-Pacific Warm Pool and adjacent land at the Last Glacial Maximum, *Global Planet. Change*, *35*, 25–35, doi:10.1016/S0921-8181(02)00089-9.

Dia, A., B. Dupré, and C. J. Allègre (1992), Nd isotopes in Indian Ocean sediments used as a tracer of supply to the ocean and circulation paths, *Mar. Geol.*, *103*, 349–359, doi:10.1016/0025-3227(92)90025-D.

Domingues, C. M., M. E. Maltrud, S. E. Wijffels, J. A. Church, and M. Tomczak (2007), Simulated Lagrangian pathways between the Leeuwin Current System and the upper-ocean circulation of the southeast Indian Ocean, *Deep Sea Res., Part II*, *54*(8–10), 797–817, doi:10.1016/j.dsr2.2006.10.003.

Ehrmann, W., G. Schmiedl, Y. Hamann, and T. Kuhnt (2007), Distribution of clay minerals in surface sediments of the Aegean Sea: A compilation, *Int. J. Earth Sci.*, *96*, 769–780, doi:10.1007/s00531-006-0119-1.

Elburg, M. A., P. Z. Vroon, B. van der Wagt, and A. Tchalikian (2005), Sr and Pb isotopic composition of five USGS glasses (BHVO-2G, BIR-1G, BCR-2G, TB-1G, NKT-1G), *Chem. Geol.*, *223*, 196–207, doi:10.1016/j.chemgeo.2005.07.001.

Erel, Y., Y. Harlavan, and J. D. Blum (1994), Lead isotope systematics of granitoid weathering, *Geochim. Cosmochim. Acta*, *58*(23), 5299–5306, doi:10.1016/0016-7037(94)90313-1.

Fagel, N. F., C. Hillaire-Marcel, and C. Robert (1997), Changes in the Western Boundary Undercurrent outflow since the Last Glacial Maximum, from smectite/illite ratios in deep Labrador Sea sediments, *Paleoceanography*, *12*(1), 79–96, doi:10.1029/96PA02877.

Fagel, N. F., C. Hillaire-Marcel, M. Humblet, R. Brasseur, D. Weis, and R. K. Stevenson (2004), Nd and Pb isotope signatures of the clay-size fraction of Labrador Sea sediments during the Holocene: Implications for the inception of the modern deep circulation pattern, *Paleoceanography*, *19*, PA3002, doi:10.1029/2003PA000993.

Fieux, M., C. Andrié, E. Charriaud, A. G. Ilahude, N. Metzl, R. Molcard, and J. C. Swallow (1996), Hydrological and chlorofiuoromethane measurements of the Indonesian

throughflow entering the Indian Ocean, *J. Geophys. Res.*, *101*(C5), 12,433–12,454, doi:10.1029/96JC00207.

Franzese, A. M., S. R. Hemming, and S. L. Goldstein (2009), Use of strontium isotopes in detrital sediments to constrain the glacial position of the Agulhas Retroflection, *Paleoceanography*, *24*, PA2217, doi:10.1029/2008PA001706.

Gingele, F. X., P. De Deckker, and C.-D. Hillenbrand (2001a), Clay mineral distribution in surface sediments between Indonesia and NW Australia—Source and transport by ocean currents, *Mar. Geol.*, *179*, 135–146, doi:10.1016/S0025-3227(01)00194-3.

Gingele, F. X., P. De Deckker, and C.-D. Hillenbrand (2001b), Late Quaternary fluctuations of the Leeuwin Current and palaeoclimates on the adjacent land masses: Clay mineral evidence, *Aust. J. Earth Sci.*, *48*, 867–874, doi:10.1046/j.1440-0952.2001.00905.x.

Godfrey, J. S. (1996), The effect of the Indonesian throughflow on ocean circulation and heat exchange with the atmosphere: A review, *J. Geophys. Res.*, *101*(C5), 12,217–12,237, doi:10.1029/95JC03860.

Goldstein, S. L., R. K. O'Nions, and P. J. Hamilton (1984), A Sm-Nd isotopic study of atmospheric dusts and particulates from major river systems, *Earth Planet. Sci. Lett.*, *70*, 221–236, doi:10.1016/0012-821X(84)90007-4.

Gordon, A. L., R. F. Weiss, W. M. Smethie, and M. J. Warner (1992), Thermocline and intermediate water communication between the South Atlantic and Indian oceans, *J. Geophys. Res.*, *97*(C5), 7223–7240, doi:10.1029/92JC00485.

Hamilton, W. (1979), Tectonics of the Indonesian region, *U.S. Geol. Surv. Prof. Pap.*, *1078*, 1–345.

Harlavan, Y., Y. Erel, and J. D. Blum (1998), Systematic changes in lead isotopic composition with soil age in glacial granitic terrains, *Geochim. Cosmochim. Acta*, *62*(1), 33–46, doi:10.1016/S0016-7037(97)00328-1.

Harrison, S. P. (1993), Late Quaternary lake-level changes and climates of Australia, *Quat. Sci. Rev.*, *12*, 211–231, doi:10.1016/0277-3791(93)90078-Z.

Hartono, H. M. S. (1990), Late Cenozoic tectonic development of the southeast Asian continental margin in the Banda Sea area, *Tectonophysics*, *181*, 267–276, doi:10.1016/0040-1951(90)90020-9.

Hesse, P. P., and G. H. McTainsh (2003), Australian dust deposits: Modern processes and the Quaternary record, *Quat. Sci. Rev.*, *22*, 2007–2035, doi:10.1016/S0277-3791(03)00164-1.

Horwitz, E. P., R. Chiarizia, and M. L. Dietz (1992), A novel strontium-selective extraction chromatographic resin, *Solvent Extr. Ion Exch.*, *10*(2), 313–336, doi:10.1080/07366299208918107.

Jeandel, C., D. Thouron, and M. Fieux (1998), Concentrations and isotopic compositions of neodymium in the eastern Indian Ocean and Indonesian straits, *Geochim. Cosmochim. Acta*, *62*(15), 2597–2607, doi:10.1016/S0016-7037(98)00169-0.

Johnson, D. (2005), *The Geology of Australia*, Cambridge Univ. Press, Cambridge, U. K.

Karas, C., D. Nürnberg, A. K. Gupta, R. Tiedemann, K. Mohan, and T. Bickert (2009), Mid-Pliocene climate change amplified by a switch in Indonesian subsurface throughflow, *Nat. Geosci.*, *2*(6), 434–438, doi:10.1038/ngeo520.

Kawamura, H., A. Holbourn, and W. Kuhnt (2006), Climate variability and land–ocean interactions in the Indo Pacific Warm Pool: A 460-ka palynological and organic geochemical record from the Timor Sea, *Mar. Micropaleontol.*, *59*, 1–14, doi:10.1016/j.marmicro.2005.09.001.

Lugmair, G. W., and S. J. G. Galer (1992), Age and isotopic relationships among the angrites Lewis Cliff 86010 and Angra dos Reis, *Geochim. Cosmochim. Acta*, *56*, 1673–1694, doi:10.1016/0016-7037(92)90234-A.

Macdonald, A. M., and C. Wunsch (1996), An estimate of global ocean circulation and heat fluxes, *Nature*, *382*, 436–439, doi:10.1038/382436a0.

Martinez, J. I., P. De Deckker, and T. T. Barrows (1999), Palaeoceanography of the last glacial maximum in the eastern Indian Ocean: Planktonic foraminiferal evidence, *Palaeogeogr. Palaeoclimatol. Palaeoecol.*, *147*, 73–99, doi:10.1016/S0031-0182(98)00153-9.

Martinson, D. G., N. G. Pisias, J. D. Hays, J. Imbrie, T. C. Moore, and N. J. Shackleton (1987), Age dating and the orbital theory of the ice ages: Development of a high-resolution 0 to 300,000-year chronostratigraphy, *Quat. Res.*, *27*(1), 1–29, doi:10.1016/0033-5894(87)90046-9.

Mohtadi, M., A. Lückge, S. Steinke, J. Groeneveld, D. Hebbeln, and N. Westphal (2010), Late Pleistocene surface and thermocline conditions of the eastern tropical Indian Ocean, *Quat. Sci. Rev.*, *29*, 887–896, doi:10.1016/j.quascirev.2009.12.006.

Murgese, D. S., and P. De Deckker (2007), The late Quaternary evolution of water masses in the eastern Indian Ocean between Australia and Indonesia, based on benthic foraminifera faunal and carbon isotopes analyses, *Palaeogeogr. Palaeoclimatol. Palaeoecol.*, *247*, 382–401, doi:10.1016/j.palaeo.2006.11.002.

Okada, H., and P. E. Wells (1997), Late Quaternary nannofossil indicators of climate change in two deep-sea cores associated with the Leeuwin Current off Western Australia, *Palaeogeogr. Palaeoclimatol. Palaeoecol.*, *131*, 413–432, doi:10.1016/S0031-0182(97)00014-X.

Olley, J. M., P. De Deckker, R. G. Roberts, L. K. Fifield, H. Yoshida, and G. Hancock (2004), Optical dating of deep-sea sediments using single grains of quartz: A comparison with radiocarbon, *Sediment. Geol.*, *169*, 175–189, doi:10.1016/j.sedgeo.2004.05.005.

Petschick, R., G. Kuhn, and F. X. Gingele (1996), Clay mineral distribution in surface sediments of the South Atlantic: Sources, transport, and relation to oceanography, *Mar. Geol.*, *130*, 203–229, doi:10.1016/0025-3227(95)00148-4.

Schmitz, W. J. (1995), On the interbasin-scale thermohaline circulation, *Rev. Geophys.*, *33*(2), 151–173, doi:10.1029/95RG00879.

Spooner, M. I., T. T. Barrows, P. De Deckker, and M. Paterne (2005), Palaeoceanography of the Banda Sea, and late Pleistocene initiation of the Northwest Monsoon, *Global Planet. Change*, *49*, 28–46, doi:10.1016/j.gloplacha.2005.05.002.

Takahashi, K., and H. Okada (2000), The paleoceanography for the last 30,000 years in the southeastern Indian Ocean by means of calcareous nannofossils, *Mar. Micropaleontol.*, *40*, 83–103, doi:10.1016/S0377-8398(00)00033-5.

Tanaka, T., et al. (2000), JNdi-1: A neodymium isotopic reference in consistency with LaJolla neodymium, *Chem. Geol.*, *168*(3–4), 279–281, doi:10.1016/S0009-2541(00)00198-4.

Thiry, M. (2000), Palaeoclimatic interpretation of clay minerals in marine deposits: An outlook from the continental origin, *Earth Sci. Rev.*, *49*, 201–221, doi:10.1016/S0012-8252(99)00054-9.

van der Kaars, S., and P. De Deckker (2002), A late Quaternary pollen record from deep-sea core Fr10/95, GC17 offshore Cape Range Peninsula, northwestern Western Australia, *Rev. Palaeobot. Palynol.*, *120*, 17–39, doi:10.1016/S0034-6667(02)00075-1.

van der Kaars, S., P. De Deckker, and F. X. Gingele (2006), A 100,000-year record of annual and seasonal rainfall and temperature for northwestern Australia based on a pollen record obtained offshore, *J. Quat. Sci.*, *21*(8), 879–889, doi:10.1002/jqs.1010.

von Blanckenburg, F., and T. F. Nägler (2001), Weathering versus circulation-controlled changes in radiogenic isotope tracer composition of the Labrador Sea and North Atlantic Deep Water, *Paleoceanography*, *16*(4), 424–434, doi:10.1029/2000PA000550.

Vroon, P. Z., M. J. van Bergen, G. L. Klaver, and W. M. White (1995), Strontium, neodymium, and lead isotopic and trace-element signatures of the East Indonesian sediments: Provenance and implications for Banda Arc magma genesis, *Geochim. Cosmochim. Acta*, *59*(12), 2573–2598, doi:10.1016/0016-7037(95)00151-4.

Wang, P. (1999), Response of Western Pacific marginal seas to glacial cycles: Paleoceanographic and sedimentological features, *Mar. Geol.*, *156*, 5–39, doi:10.1016/S0025-3227(98)00172-8.

Wells, P. E., and G. M. Wells (1994), Large-scale reorganization of ocean currents offshore Western Australia during the late Quaternary, *Mar. Micropaleontol.*, *24*, 157–186, doi:10.1016/0377-8398(94)90020-5.

Wijffels, S. E., G. Meyers Hautala, and W. M. L. Morawitz (1996), The WOCE Indonesian Throughflow repeat hydrography sections: I10 and IR6, *International WOCE Newsletter*, *24*, 25–28.

Williams, M., E. Cook, S. van Der Kaars, T. T. Barrows, J. Shulmeister, and P. Kershaw (2009), Glacial and deglacial climatic patterns in Australia and surrounding regions from 35,000 to 10,000 years ago reconstructed from terrestrial and near-shore proxy data, *Quat. Sci. Rev.*, *28*(23–24), 2398–2419, doi:10.1016/j.quascirev.2009.04.020.

Wyrtki, K. (1962), The upwelling in the region between Java and Australia during the South-East monsoon, *Aust. J. Mar. Freshwater Res.*, *13*, 217–225, doi:10.1071/MF9620217.

Wyrwoll, K.-H., and G. H. Miller (2001), Initiation of the Australian summer monsoon 14,000 years ago, *Quat. Int.*, *83–85*, 119–128, doi:10.1016/S1040-6182(01)00034-9.

Yokoyama, Y., P. De Deckker, K. Lambeck, P. Johnston, and L. K. Fifield (2001), Sea-level at the Last Glacial Maximum: Evidence from northwestern Australia to constrain ice volumes for oxygen isotope stage 2, *Palaeogeogr. Palaeoclimatol. Palaeoecol.*, *165*, 281–297, doi:10.1016/S0031-0182(00)00164-4.

Zuraida, R., A. Holbourn, D. Nürnberg, W. Kuhnt, A. Dürkop, and A. Erichsen (2009), Evidence for Indonesian throughflow slowdown during Heinrich events 3–5, *Paleoceanography*, *24*, PA2205, doi:10.1029/2008PA001653.